A Novel Highly Integrated Hybrid Energy Storage System for Electric Propulsion and Smart Grid Applications

Alessandro Serpi, Mario Porru and Alfonso Damiano

Additional information is available at the end of the chapter

Abstract

This chapter addresses potentialities and advantages of a highly integrated hybrid energy storage system (HESS) for electric propulsion and smart grids. This configuration consists of a highly integrated battery-ultracapacitor system (HIBUC) and aims to benefit from the advantages of both passive and active HESS configurations. Particularly, the integration of the ultracapacitor module (UM) within the DC-link of the DC/AC multilevel converter enables the decoupling between DC-link voltage and energy content without the need for any additional DC/DC converter. As a result, HIBUC benefits from simplicity and energy flow management capabilities very similar to those achieved by passive and active HESS configurations, respectively. This is highlighted properly by a theoretical analysis, which also accounts for a comparison between HIBUC and both passive and active HESS configurations. Some HIBUC application examples are also reported, which highlight the flexibility and potentialities of HIBUC for both electric propulsion systems and smart grids.

Keywords: batteries, energy management, energy storage, electric vehicles, modeling, smart grids, supercapacitors, ultracapacitors

1. Introduction

Electric energy storage systems (ESSs) are widely recognized as one of the most promising technology for enabling the transition toward a sustainable energy system [1–3]. Particularly, transportation electrification is pushing toward progressive improvements of ESS technologies, especially for light- and heavy-road electric vehicles: these have to rely on on-board ESSs

for guaranteeing long mileage and short charging time. Consequently, high efficiency, low costs, small volumes, and weights are desirable. The employment of ESSs is increasingly considered also for such systems that have been propelled electrically since a long time, such as railway and ships, in order to increase system efficiency and fuel economy, as well as ensuring reliable operation of on-board power systems [4–6]. In this context, both hybrid and all-electric ships are expected to be appealing in the forthcoming future. Similarly, ESSs are a key point for designing more electric aircrafts, in which pneumatic and hydraulic actuators are being replaced with electrical ones [7]. Therefore, on-board ESSs should start the engines, maintain DC-link voltage constant over dynamic operations, and, above all, guarantee emergency power supply. ESSs can be employed successfully also for addressing several issues affecting modern power systems, such as reduced level of power quality, massive growth of distributed generation, and high penetration of renewable energy sources [8–10]. Particularly, integrating the massive and increasing share of photovoltaic and wind power plants installed all over the world is one of the main challenges for future power systems, which will be faced resorting to smart grid and microgrid concepts. In this context, ESSs are the ideal solution for mitigating power fluctuations, storing overproduction, and releasing it when required, improving overall reliability and power quality.

An ESS consists of two main stages, i.e., the power conversion system and the energy storage unit, as shown in **Figure 1**. The power conversion system is generally represented by a power electronic converter, which has to regulate ESS voltage and current levels in order to match application requirements. Whereas, the energy conversion occurs within the energy storage unit, which exchange electrical energy only, storing it into different forms (mechanical, chemical, magnetic, etc.).

There are several ESSs available on the market, which are generally classified in accordance with their energy/power density (Wh/l, W/l) or specific energy/power (Wh/Kg, W/Kg), as highlighted in **Figure 2** [11, 12]. High-energy density ESSs are able to provide large amount of energy but over long time periods, as occurring for the majority of electrochemical batteries. These are the first ESS introduced on the market and still represent the most widespread. Electrochemical batteries can be further classified based on the chemical reaction they exploit. Lead acid (PbA) is probably the most-known technology; it is being widely used on vehicles for starting, lighting, and ignition purposes. PbA batteries are currently employed when sizes and weights are not an issue, such as isolated power systems and UPSs, whereas, lithium-ion
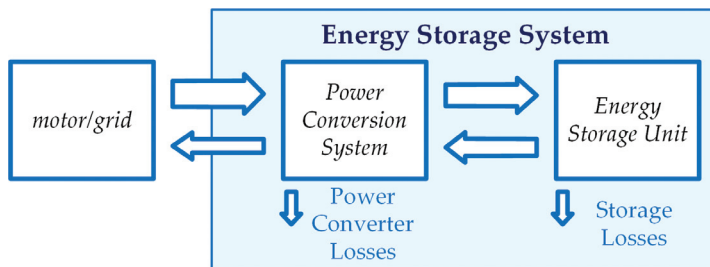

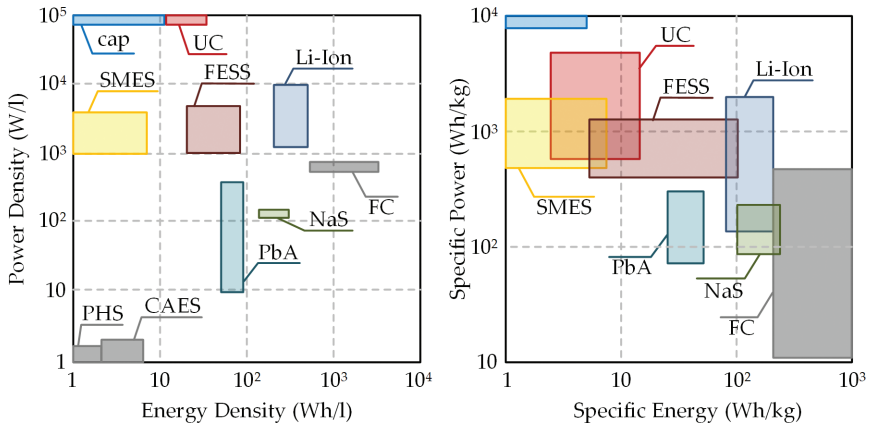**Figure 1.** ESS schematic representation.

Figure 2. Energy/power density (left) and specific energy/power (right) of ESSs on Ragone plots: pumped hydroelectric storage system (PHS), compressed air energy storage system (CAES), and fuel cell (FC).

batteries (Li-ion) are surely the best solution for modern electric vehicles due to their very high-energy density and specific energy. However, sodium-based batteries may be preferred when high capacity is required, namely for load leveling and renewable energy sources integration. Despite their advantages, electrochemical batteries generally suffer from low power capabilities; thus, even if research is focused on improving power density, they are not yet the best solution for high-power applications [13, 14].

Differently from electrochemical batteries, high-power density ESSs can provide much little amount of energy but in very short times, which is the case of flywheel energy storage system (FESS), superconducting magnetic energy storage system (SMES), and ultracapacitors (UCs). Particularly, FESS is characterized by very high efficiency, long life expectancy, and low environmental impact. However, it presents a quite high self-discharge rate and also suffers from safety issues as far as high speeds are concerned [15–17]. Regarding SMES, a cryogenic system ensures the superconducting state of coils. Consequently, losses are due to power converters only, leading to a very high overall efficiency. Other advantages consist of fast response and wide power range, as well as long lifespan. Nevertheless, SMES is very expensive due to the high costs of both superconductors and cryogenic system; thus, although it has been recently tested for power quality and voltage stabilization in both transmission and distribution systems, it is still employed in military applications mostly [18–20]. The main advantages of UCs are high-power capability, quite long life cycle and no memory effect, but they cannot store great amount of energy unless big and costly UC modules are used. Thus, UCs have been used for power quality applications and for handling small regenerative braking on electric propulsion systems [21–23].

Based on the previous considerations, it can be stated that a single ESS technology hardly matches both energy and power application requirements. Particularly, electrochemical batteries are very suitable for providing energy services, in which high-energy storage capability is mandatory. On the other hand, FESS, SMES, and UCs are more appropriate for power services,

when high-power rates are required for very short times. In addition, further constraints may regard efficiency, life cycle, and cost, which might make one ESS technology unsuitable. In this regard, a viable and promising solution is the employment of a hybrid energy storage system (HESS), which consists of combining high-energy and high-power density ESSs in order to benefit from the advantages of different ESS technologies [24–27]. As a result, HESS may bring increased performances, higher efficiency, longer lifetime, reduced costs, and more appropriate design and sizing. Among all the ESS combinations, HESSs made up of electrochemical batteries and UCs are the most popular and promising solutions because of the perfect complementarity between their features [28–30].

Consequently, this chapter focuses on HESS made up of a battery pack (BP) and an ultracapacitor module (UM). Particularly, a brief overview of main HESS configurations and management approaches is provided in Section 2. Then, Section 3 focuses on a highly integrated HESS configuration [31–33], in which BP and UM are coupled only by means of a multilevel converter. This highly integrated battery-ultracapacitor system (HIBUC) is also compared to those described in Section 2, highlighting its most important advantages. In Section 3, two HIBUC application examples are also presented and discussed based on numerical simulations. Concluding remarks are reported in Section 4.

2. Overview on hybrid energy storage systems

Considering a hybrid energy storage system (HESS) made up of a battery pack (BP) and an ultracapacitor module (UM), a number of configurations have been proposed in the literature, which differ from each other mainly due to the number of power electronic converters involved. Particularly, no or few power electronic converters entail simple configurations, but poor flexibility and energy management. As the number of power electronic converters increases, energy management capability, and, thus, HESS exploitation increase, but at the cost of increased complexity, costs, volumes, and weights. The following sections investigate the most important HESS configurations, as well as their management and control strategies, by highlighting their most important advantages and drawbacks.

2.1. HESS configurations

HESS configurations can be roughly classified into passive and active configurations; in passive HESS, BP and UM are directly coupled to the DC-link of the DC/AC converter, as depicted in **Figure 3** [34, 35]. Therefore, BP and UM share the same voltage, which generally varies with BP state-of-charge. As a result, UM voltage cannot vary independently, resulting in its poor energy exploitation. Still referring to **Figure 3**, the following relationships can be introduced:

$$V_b = r_b i_b + L \frac{di_b}{dt} + V_{DC} \tag{1}$$

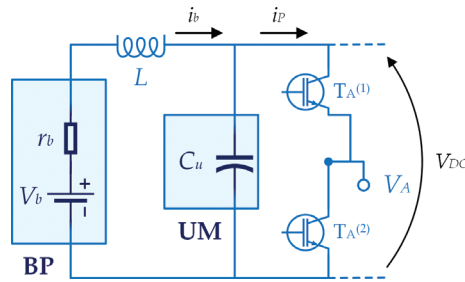$$C_u \frac{dV_u}{dt} = i_b - i_P. \tag{2}$$

Figure 3. Schematic representation of passive HESS configuration.

Particularly, a simple but effective BP model has been considered, which consists of a voltage source V_b series-connected with an internal resistance r_b, while i_b is the battery current. BP is coupled to the DC-link through an inductive filter, whose inductance L should prevent i_b from unsuitable sudden variations, V_{DC} being the DC-link voltage. Referring to Eq. (2), C_u denotes the capacitance of the UM, whereas i_P denotes the power current, which is proportional to the power drawn or delivered by the DC/AC converter. The DC-link energy content E_{DC} and its time-variation can be expressed, respectively, as:

$$E_{DC} = \frac{1}{2} C_u V_{DC}^2 \tag{3}$$

$$\frac{dE_{DC}}{dt} = V_{DC}(i_b - i_P). \tag{4}$$

The comparison between Eq. (2) and Eq. (4) reveals a significant coupling between E_{DC} and V_{DC}, which cannot be varied within a wide range. This results in a poor UM exploitation, as well as in an unsuitable energy management, which are the main drawbacks of this HESS configuration. Consequently, in spite of its simplicity and cheapness, passive HESS configuration is rarely used due to weak performances that make it not suitable for most applications.

Much better performances can be achieved by semi-active and active HESS configurations, which exploit one or more DC/DC converters for decoupling BP and UM [36–43]. Particularly, **Figure 4** shows an active parallel configuration, in which BP and UM are parallel-connected to the DC-link both through DC/DC converters. Referring to this configuration, the following relationships can be introduced:

$$\tilde{V}_b = L\frac{d\tilde{i}_b}{dt} + V_{DC} \ , \quad C\frac{dV_{DC}}{dt} = \tilde{i}_b + \tilde{i}_u - i_P \tag{5}$$

in which, C is the capacitance of the DC-link, which is much smaller than C_u. Whereas

$$\tilde{V}_b = \frac{1}{k_b}(V_b - r_b i_b) \ , \quad \tilde{i}_b = k_b i_b \tag{6}$$

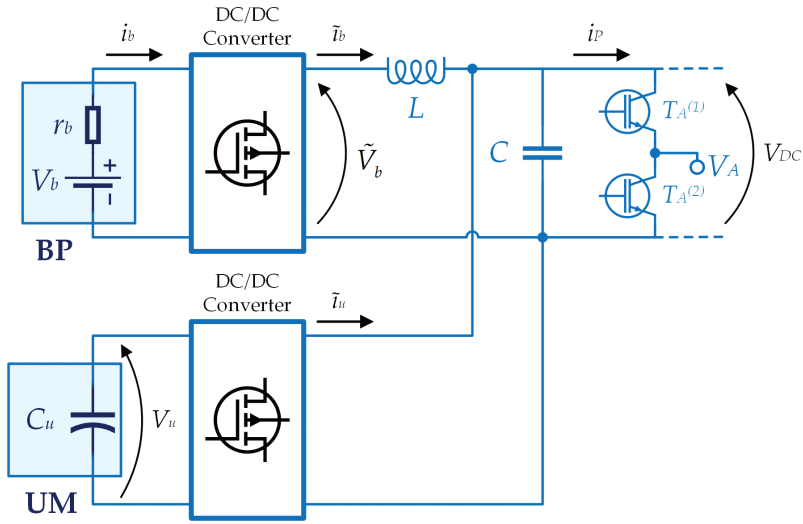$$V_{DC} = \frac{1}{k_u}V_u \ , \quad \tilde{i}_u = -k_u C_u \frac{dV_u}{dt}. \tag{7}$$

Figure 4. Schematic representation of active parallel HESS configuration.

Particularly, Eqs. (6) and (7) have been achieved by assuming ideal DC/DC converters, which have been modeled by simple gains (k_b and k_u for BP and UM, respectively). Therefore, the combination of Eq. (5) with Eqs. (6) and (7) leads to the following expressions:

$$V_b = r_b i_b + k_b^2 L \frac{d i_b}{dt} + k_b V_{DC} \tag{8}$$

$$C \frac{d V_{DC}}{dt} = k_b i_b - k_u C_u \frac{d V_u}{dt} - i_P. \tag{9}$$

Regarding the DC-link energy content, it should account not only for C, but also for C_u in order to make the comparison with all HESS configurations consistent. Consequently, E_{DC} and its time derivative can be expressed as

$$E_{DC} = \frac{1}{2} C V_{DC}^2 + \frac{1}{2} C_u V_u^2 \tag{10}$$

$$\frac{d E_{DC}}{dt} = V_{DC}(k_b i_b - i_P). \tag{11}$$

Therefore, considering both Eqs. (9) and (11), it can be seen that V_{DC} and E_{DC} can be controlled independently by setting the duty cycles of the DC/DC converters properly. However, Eqs. (9) and (11) are characterized by increased complexity compared to passive HESS configurations. Furthermore, these equations highlight a significant coupling among all system variables, which makes control system design a not trivial issue. Consequently, advanced management and control systems are required in order to exploit active HESS configurations properly.

2.2. HESS management and control

As far as semi-active or active HESS configurations are concerned, the management and control system cover a fundamental role for exploiting the HESS at the maximum extent. Particularly, an appropriate selection of HESS management strategy is of paramount importance, even from the design stage, especially for sizing BP and UM properly in accordance with target performances, and technical and economic constraints. It is fundamental also for assuring HESS efficiency, reliability, and durability.

Referring to **Figure 5**, HESS management consists mainly of a sharing criterion for splitting the overall HESS energy flow between BP and UM. Literature review reveals that several approaches have been proposed in order to exploit BP and UM inherent features to the maximum extent, preventing them from unsuitable operation as well. In this regard, UM generally handles fast power fluctuations, whereas BP copes with the average power demand. This principle is the basis of the simplest HESS management strategy known as frequency-based management (FBM); this consists of splitting the overall power demand into high- and low-frequency components, which have to be tracked by UM and BP, respectively [44, 45]. An alternative approach is the so-called rule-based management (RBM), which exploits the single ESSs in accordance with an appropriate order of priority by means of a pre-set of rules [46, 47]. In this regard, it is worth noting that FBM and RBM may be combined to each other or with fuzzy logic algorithms in order to account for ESS constraints and to improve overall HESS performances [48–51].

Although FBM and RBM are intuitive, simple, and easy to implement, they generally do not lead to optimal solutions. For this reason, another popular approach is determining BP and UM reference power profiles by minimizing suitable cost functions over a given time horizon. Hence, different optimal solving techniques can be used, such as model predictive control, mixed-integer/linear programming, nonlinear programming, and dynamic programming [52–55]. However, such solving techniques are generally complex to implement and quite time-demanding. Consequently, heuristic approaches have been also proposed, like genetic algorithms and particle swarm optimization, which achieve sub-optimal solutions but faster and with less computational efforts [56–58]. As a result, very complex and sophisticated cost functions can be considered, which can account for many system constraints and goals. The
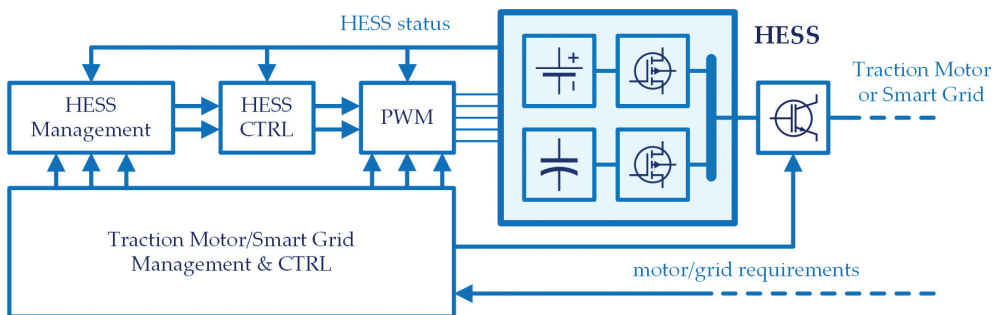

Figure 5. Schematic representation of an HESS management and control system.

main advantage of these approaches consists of enabling HESS to provide multiple services in an optimal manner, by both economic and technical points of view; this aspect makes HESS very competitive, especially for smart grid applications.

3. A novel highly integrated HESS

In order to overcome the issues arising from both passive and active HESS configurations, a highly integrated solution has been proposed by the authors in [31–33], whose schematic representation is depicted in **Figure 6**. It consists of coupling a BP with an UM through a multilevel converter, namely a three-level neutral-point-clamped converter (NPC). The key feature of the proposed highly integrated battery-ultracapacitor system (HIBUC) is the full integration of UM within the DC-link of the NPC, which decouples the overall DC-link voltage (V_{DC}) from its energy content (E_{DC}). As a result, HIBUC energy flow management is quite similar to that achieved with active HESS configurations without resorting to any DC/DC converter, as detailed in the following sections.

3.1. HIBUC modeling

Still referring to **Figure 6**, the DC-link of HIBUC is split into high-side and low-side due to the three-level configuration: high-side consists of the UM, whose overall voltage and capacitance are denoted by V_u and C_u, respectively, while the low-side is made up of conventional capacitors, V and C being the corresponding voltage and capacitance. Hence, HIBUC main equations can be expressed as

$$V_b = r_b\, i_b + L\frac{di_b}{dt} + V_{DC}\ ,\quad V_{DC} = V_u + V \tag{12}$$

$$C_u \frac{dV_u}{dt} = i_b - i_H\ ,\quad C\frac{dV}{dt} = i_b - i_L. \tag{13}$$
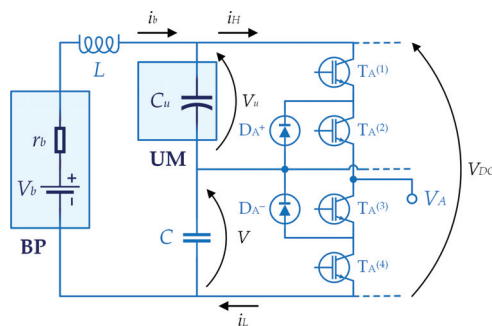

Figure 6. The highly integrated HESS configuration proposed in [31–33].

Whereas, the overall DC-link energy content can be determined easily as

$$E_{DC} = \frac{1}{2} C_u V_u^2 + \frac{1}{2} C V^2. \tag{14}$$

Based on both Eqs. (12) and (13), the dynamic equation of the DC-link voltage can be achieved as

$$C_{DC} \frac{dV_{DC}}{dt} = i_b - i_{DC} \; , \quad C_{DC} = \frac{C_u C}{C_u + C} \; , \quad i_{DC} = \frac{C}{C_u + C} i_H + \frac{C_u}{C_u + C} i_L \tag{15}$$

where C_{DC} and i_{DC} are defined as the equivalent DC-link capacitance and current, respectively. Furthermore, by time-differentiating Eq. (14) and combining the result with (13), the following relationship is achieved:

$$\frac{dE_{DC}}{dt} = V_{DC}(i_b - i_P) \; , \quad i_P = \frac{V_u}{V_{DC}} i_H + \frac{V}{V_{DC}} i_L. \tag{16}$$

Hence, Eq. (16) reveals that E_{DC} depends on both i_b and i_P. However, since the latter is generally imposed by the application requirements, E_{DC} can be regulated successfully through i_b only, while V_{DC} can be driven independently by means of i_{DC}, as pointed out by Eq. (15). This occurs as far as i_{DC} and i_P differ from each other. Otherwise, both V_{DC} and E_{DC} time variations would be proportional to the difference between i_b and i_P, thus E_{DC} and V_{DC} control decoupling cannot be achieved. Therefore, considering both Eqs. (15) and (16), the following relationship can be introduced:

$$\begin{bmatrix} i_{DC} \\ i_P \end{bmatrix} = A \cdot \begin{bmatrix} i_H \\ i_L \end{bmatrix} \; , \quad A = \begin{bmatrix} \dfrac{C}{C_u + C} & \dfrac{C_u}{C_u + C} \\ \dfrac{V_u}{V_{DC}} & \dfrac{V}{V_{DC}} \end{bmatrix} \tag{17}$$

Consequently, since A must be non-singular, the following constraint is achieved:

$$CV - C_u V_u \neq 0 \tag{18}$$

Hence, if Eq. (18) is satisfied, i_{DC} and i_P can differ from each other; this does not occur in conventional NPC configurations, which are characterized by equal voltages and capacitances. Whereas, HIBUC suitably exploits DC-link capacitance and voltage unbalances, leading to a decoupled control of V_{DC} and E_{DC}.

3.1.1. Comparison with passive and active HESS configurations

In order to highlight the advantages of HIBUC compared to passive and active HESS configurations, reference can be made to the per unit DC-link energy content (e_{DC}), which is defined as follows:

$$e_{DC} = \frac{E_{DC}}{\frac{1}{2} C V_{DC}^2} \tag{19}$$

Hence, considering Eqs. (3), (10), and (14), the following results are achieved:

$$e_{DC}^{(P)} = \alpha \ , \quad \alpha = \frac{C_u}{C}$$

(20)

$$e_{DC}^{(A)} = 1 + \alpha\,\xi^2 \ , \quad \xi = \frac{V_u}{V_{DC}} = k_u$$

(21)

$$e_{DC}^{(H)} = \alpha \cdot \xi^2 + (1 - \xi)^2 \ , \quad \xi = \frac{V_u}{V_{DC}}$$

(22)

where the superscripts (P), (A), and (H) denote passive, active and HIBUC configuration, respectively. In addition, α is the capacitance factor, which is much greater than 1 because C_u is much greater than C. Furthermore, ξ is the UM voltage share, which is equal to k_u in the case of active HESS configuration. It is worth noting that ξ ranges from 0 to 1 for the HIBUC configuration and that the same reasonably occurs also for active HESS configurations.

Hence, considering the e_{DC} evolutions with ξ depicted in **Figure 7**, different considerations can be made for each HESS configuration and for a given α value. Particularly, referring to passive HESS configuration at first, e_{DC} does not depend on ξ, as already pointed out by Eq. (20). This is because the voltage across UM always equals V_{DC}, thus $\xi = 1$ over any operating conditions. As a consequence, once α has been set, E_{DC} can vary only with V_{DC}. However, since V_{DC} should be kept almost constant in order to supply the converter properly, a poor UM exploitation is achieved, as expected.

Considering now active HESS configuration, minimum and maximum e_{DC} values are always achieved for $\xi = 0$ and $\xi = 1$, respectively, as pointed out in the following:

$$\breve{\xi} = 0 \qquad \rightarrow \qquad \breve{e}_{DC}^{(A)} = \min_{0 \le \xi \le 1}\left\{e_{DC}^{(A)}\right\} = 1$$

(23)

$$\widehat{\xi} = 1 \qquad \rightarrow \qquad \widehat{e}_{DC}^{(A)} = \max_{0 \le \xi \le 1}\left\{e_{DC}^{(A)}\right\} = 1 + \alpha$$

(24)

Therefore, the maximum exploitation of the DC-link energy content can be achieved by varying ξ within [0,1] as

$$\Delta\xi = \widehat{\xi} - \breve{\xi} = 1 \qquad \rightarrow \qquad \Delta e_{DC}^{(A)} = \widehat{e}_{DC}^{(A)} - \breve{e}_{DC}^{(A)} = \alpha$$

(25)

Hence, differently from passive HESS configuration, active configuration enables the DC-link energy content to vary with ξ without the need of changing V_{DC}. However, it is worth noting that the operating range of ξ is much narrower than [0,1] because ξ equals k_u, which is constrained by DC/DC converter maximum and minimum duty cycle capabilities.

Focusing now on the HIBUC configuration, the minimum e_{DC} value is achieved in correspondence of the following ξ value:

$$\breve{\xi} = \frac{1}{1 + \alpha} \qquad \rightarrow \qquad \breve{e}_{DC}^{(H)} = \min_{0 \le \xi \le 1}\left\{e_{DC}^{(H)}\right\} = \frac{\alpha}{1 + \alpha}$$

(26)

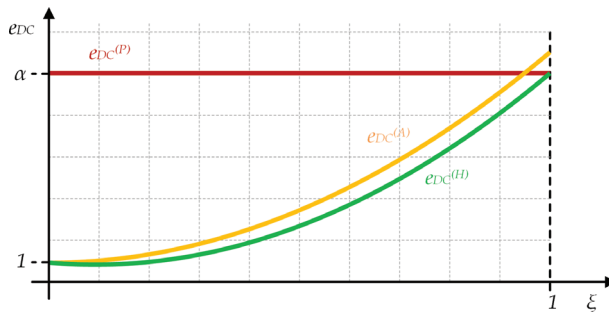**Figure 7.** The e_{DC} evolutions with ξ for $\alpha = 10$: passive, active, and HIBUC configurations.

Whereas, given that α is greater than 1, the maximum e_{DC} value is reached for $\xi = 1$, as pointed out in the following:

$$\widehat{\xi} = 1 \qquad \rightarrow \qquad \widehat{e}_{DC}^{(H)} = \max_{0 \le \xi \le 1} \left\{ e_{DC}^{(H)} \right\} = \alpha \tag{27}$$

Consequently, maximum exploitation of the DC-link energy content is achieved if ξ varies as follows:

$$\Delta\xi = \widehat{\xi} - \widecheck{\xi} = \frac{\alpha}{1 + \alpha} \qquad \rightarrow \qquad \Delta e_{DC}^{(H)} = \widehat{e}_{DC}^{(H)} - \widecheck{e}_{DC}^{(H)} = \frac{\alpha^2}{1 + \alpha} \tag{28}$$

The evolutions of both $\Delta\xi$ and Δe_{DC} with α are depicted in **Figure 8**. Particularly, for low α values, active HESS configuration shows superior performances compared to HIBUC, which is characterized by limited UM voltage range, and thus, poor DC-link energy exploitation. However, HIBUC performances rapidly increase with α, they becoming very close to those achieved by active HESS configurations for relatively high α values. Since α should be quite high due to the huge capacitance of UM, e.g., hundreds or even thousands, HIBUC is a very competitive solution even versus active HESS configuration because it can assure very similar performances in terms of energy flow management. In addition, HIBUC benefits also from a multilevel converter, whose increased complexity and costs are counterbalanced by improved output voltage and current waveforms due to the availability of multiple voltage levels.

3.2. HIBUC management and control

The overall HIBUC management and control scheme is depicted in **Figure 9**. The comparison with **Figure 5** reveals some differences, especially due to the high degree of integration among all HIBUC components. Particularly, the NPC has to account for HIBUC needs in terms of energy flow management, thus it cannot be driven only in accordance with application requirements. Regarding the HIBUC management block, it has to synthesize the most suitable BP current profile ($i_b{}^*$) based on the chosen HIBUC management approach; this is then tracked
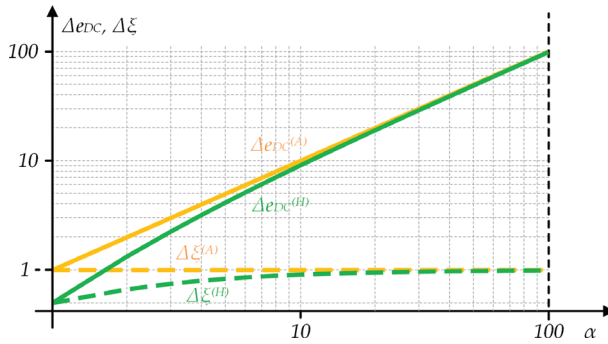
Figure 8. The evolutions of both $\Delta\xi$ (dashed lines) and Δe_{DC} (solid lines) with α: active and HIBUC configurations.
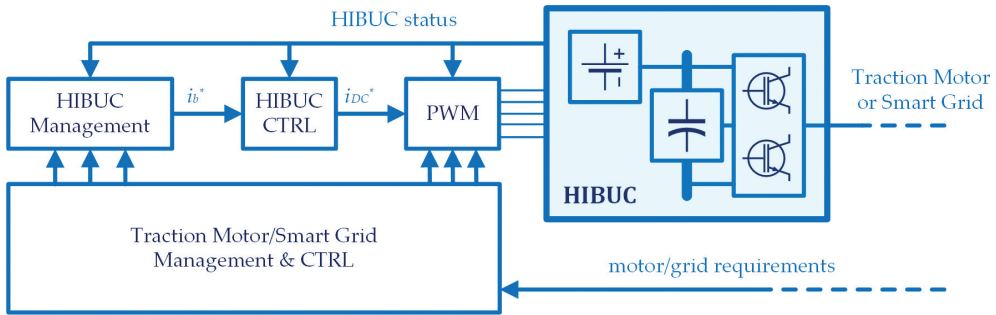

Figure 9. General overview of the HIBUC management and control scheme.

by means of the HIBUC control system, which can be designed in accordance with both Eqs. (12) and (15). As a result, a suitable i_{DC}^{*} is achieved, whose implementation is guaranteed by means of advanced PWM patterns that account for both HIBUC and application requirements, as well detailed in [33, 59, 60].

In conclusion, the structure of both HIBUC management and control blocks generally depends on the specific application, as well as on the kind of power and energy services HIBUC has to provide. For this reason, two application examples are reported in the following, for each of which a much in-depth analysis of these blocks is presented, as well as some simulation results.

3.2.1. Electric propulsion system

The HIBUC management and control blocks for the highly integrated electric propulsion system proposed in [31–33] are depicted in **Figure 10**. Focusing on the HIBUC energy management at first, the idea is to exploit the UM over acceleration and regenerative braking mainly. Consequently, the reference E_{DC} profile is set in accordance with the actual motor/vehicle speed (ω_m), namely E_{DC} should decrease properly as ω_m increases in order to enable UM to release its energy content gradually during acceleration, as well as storing it back
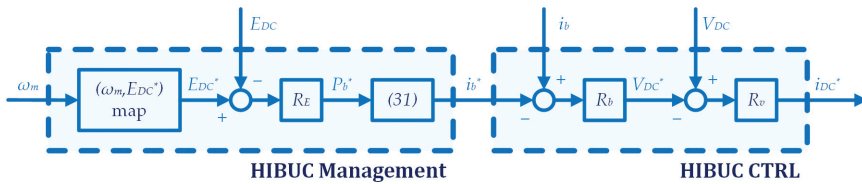
Figure 10. The HIBUC management and control scheme for an electric propulsion system.

during regenerative braking. In this regard, different maps can be chosen depending on UM sizing and on the kind of assistance it has to provide to BP in supplying the traction motor over these operating conditions, as pointed out in [32].

Once $E_{DC}*$ has been set, its tracking can be accomplished through a PI regulator (R_E), which can be designed in accordance with Eq. (16), but expressed as

$$\frac{dE_{DC}}{dt} = P_b - P_P \ , \quad P_b = V_{DC}i_b \ , \quad P_P = V_{DC}i_P. \tag{29}$$

Then, in order to overcome the dependence of P_b from V_{DC}, it is possible to multiply (12) by i_b and substituting the result in Eq. (29), leading to the following expression:

$$P_b = i_b(V_b - r_b \, i_b) - \frac{1}{2}L\frac{di_b^2}{dt} \simeq i_b(V_b - r_b \, i_b) \tag{30}$$

in which, the magnetic energy variation related to the inductive filter can be neglected safely due to the relative low inductance value. As a result, the reference i_b value can be computed as follows:

$$i_b^* = \frac{V_b}{2r_b} - \sqrt{\left(\frac{V_b}{2r_b}\right)^2 - \frac{P_b^*}{r_b}}. \tag{31}$$

Regarding the HIBUC control block, it consists of two nested control loops: the external loop regulates i_b through V_{DC} by means of a PI regulator, which can be designed easily based on Eq. (12). As a result, a reference DC-link voltage profile is achieved, whose tracking is demanded to the internal loop; this determines the most suitable reference i_{DC} profile by means of another PI regulator, which is designed in accordance with Eq. (15).

In order to highlight the effectiveness of the proposed configuration, a simulation study has been performed in MATLAB-Simulink, whose main parameters are reported in **Table 1**. While simulations results are depicted in **Figures 11**–**15**. Particularly, each variable is shown in per unit with reference to the corresponding base value shown in **Table 1**. Focusing on **Figure 11** at first, different speed profiles have been considered for simulating a start and stop of the vehicle, which are characterized by decreasing ramp times (5 s for case 1, 4 s for case 2, and 3 s for case 3). While the corresponding motor torque evolutions are depicted in **Figure 12**. The latter reveals higher torque demands as soon as faster speed variations are required, namely from case 1 to case 3, as expected. Considering the current evolutions shown in **Figure 13**, it

EPS parameters and rated values

	$T_{e,n}$	$\omega_{m,n}$	$P_{m,n}$	V_b	r_b	L_b	I_b	C_u	C
Value	110	3500	40.3	450	0.4	15	89.6	1.7	1.6
Units	Nm	rpm	kW	V	Ω	mH	A	F	mF

Table 1. Parameters and rated values of the electric propulsion system.
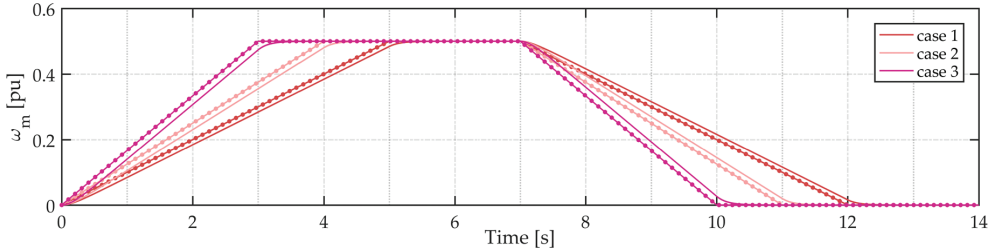
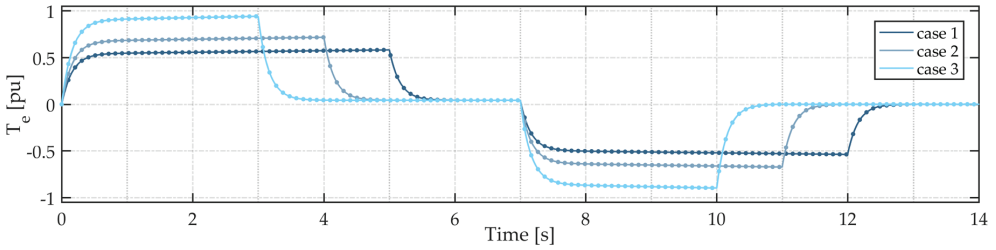**Figure 11.** Motor speed evolution achieved over vehicle start and stop.

Figure 12. Motor torque evolution achieved over vehicle start and stop.

can be seen that high power demands occur during both vehicle acceleration and braking, especially in comparison with steady state vehicle power requirements. However, BP is prevented from coping with such high and fast power variations, as proved by the low battery current profiles achieved in all cases and still shown in **Figure 13**. This is due to UM, which is discharged and charged appropriately in accordance with the (ω_m, E_{DC}^*) map, as highlighted in **Figure 14**. In addition, **Figure 15** shows that V_u is reduced during vehicle acceleration, but V is increased simultaneously. Consequently, V_{DC} can be kept sufficiently high in order to prevent unsuitable and fast BP current variations. Similar considerations can be made during regenerative braking, in correspondence of which UM is recharged, while BP current is slowly driven to zero. As a result, HIBUC enables the UM to supply the motor on its own mostly during both vehicle acceleration and regenerative braking, thus preventing BP from an unsuitable exploitation.
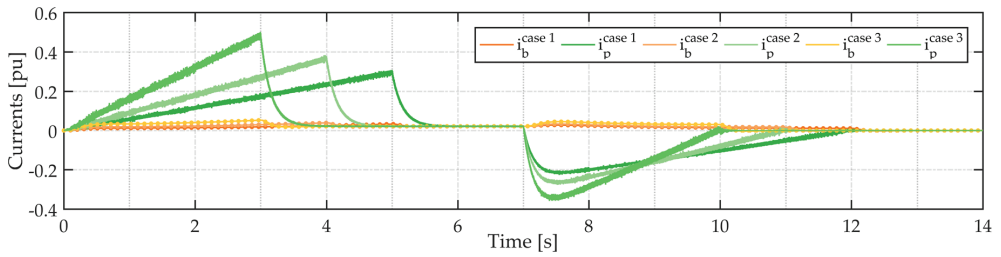
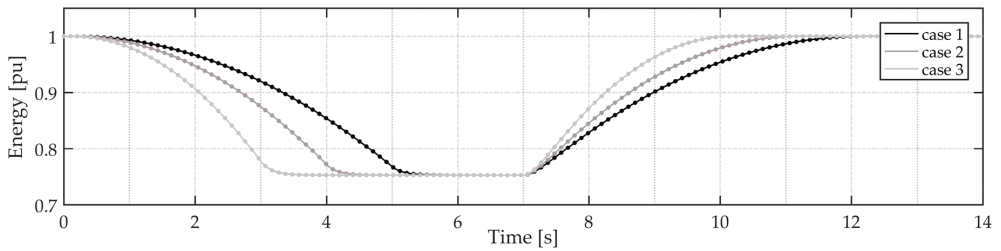**Figure 13.** Power and battery current evolutions over vehicle start and stop: i_P (green) and i_b (gold).

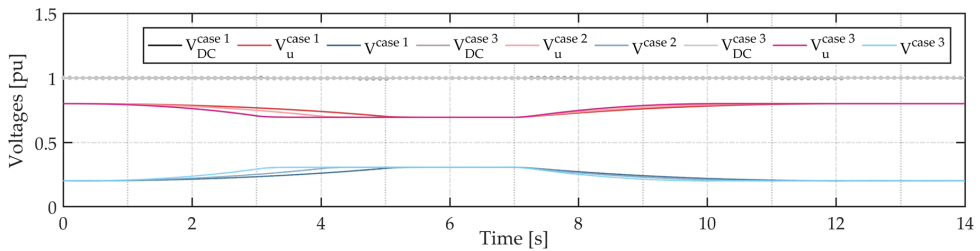**Figure 14.** DC-link energy variations over vehicle start and stop.

Figure 15. DC-link voltage evolutions over vehicle start and stop: V_{DC} (gray), V_u (red), and V (blue).

3.2.2. Smart grid

The HIBUC management and control blocks for a smart grid are depicted in **Figure 16**. Particularly, it differs from **Figure 10** only in terms of HIBUC management because the tracking of both $i_b{}^*$ and $V_{DC}{}^*$ does not depend on the specific application. Therefore, focusing on the HIBUC management only, it can be seen that a frequency-based management approach has been followed [61], namely the smart grid reference active power profile ($P_e{}^*$) is processed by an appropriate low-pass filter in order to extract low-frequency components only. These are further processed by the energy management block, which has to synthesize the reference BP
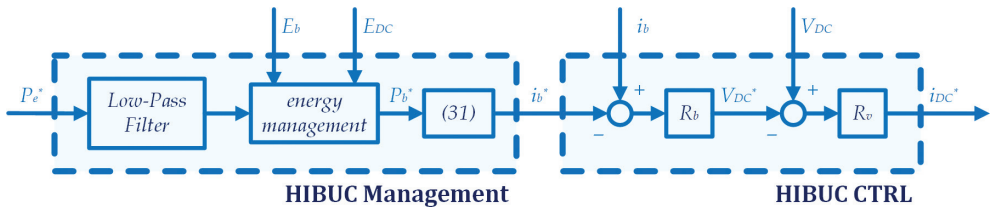
Figure 16. The HIBUC management and control scheme for a smart grid.

power profile in accordance with BP energy and power constraints. As a result, the UM has to cope with high-frequency power components only, which are generally characterized by poor energy content. However, since UM has to compensate for system losses, forecasting errors, and relatively low BP dynamic performances, the energy management block accounts also for the DC-link and, thus, the UM energy content in defining the reference BP power profile. Hence, if UM energy level is too low, additional power is delivered by BP with the aim of restoring an intermediate UM energy content. The opposite occurs when UM is almost fully charged, namely BP should draw energy from UM in order to preserve its continuous operation. As a result, the HESS configuration is exploited properly, not only by differentiating the kind of services BP and UM have to provide, but also by enabling a mutual support between the single ESSs.

A simulation study has been carried out in MATLAB-Simulink with reference to the main parameters shown in **Table 2**. Particularly, HIBUC has been sized differently from the previous application (electric propulsion system), especially in terms of voltage and capacitance ratings, in order to better match the new application requirements. Simulation results are depicted in **Figures 17–21**; all the results are expressed in per unit with reference to the corresponding base values shown in **Table 2**. Simulations refer to several active and/or reactive smart grid power variations, as highlighted in **Figure 17**. In addition, after 3 s, a noise signal has been added to the reference active power in order to test HIBUC performances in preventing BP from coping with such high-frequency power fluctuations. Still focusing on **Figure 17**, it can be seen that a very fast and suitable reference power tracking is achieved. This is mainly due to the fast UM dynamic response, while a much slower BP power response is achieved due to the employment of a low-pass filter, as highlighted in **Figure 18**. Particularly, the low-pass filter prevents BP from quickly reacting to reference active power variations, as well as from coping with the noise signal added to the reference active power; this is handled by UM on its own mostly, as still highlighted in **Figure 18**.

MG parameters and rated values

	$P_{e,n}$	V_{line}	f_{line}	V_b	r_b	L_b	I_b	C_u	C
Value	40	230	50	1000	0.4	15	40	141	0.94
Units	kW	Vrms	Hz	V	Ω	mH	A	mF	mF

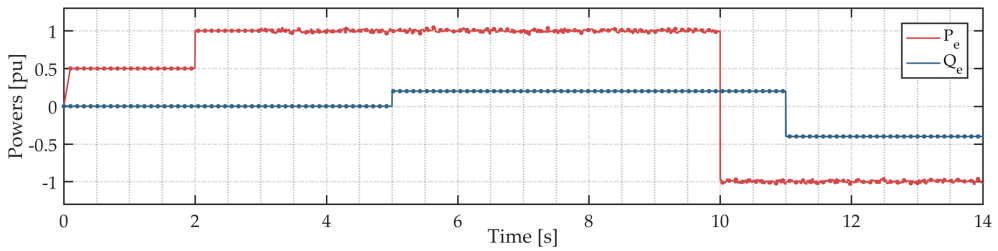**Table 2.** Parameters and rated values of the smart grid scenario.

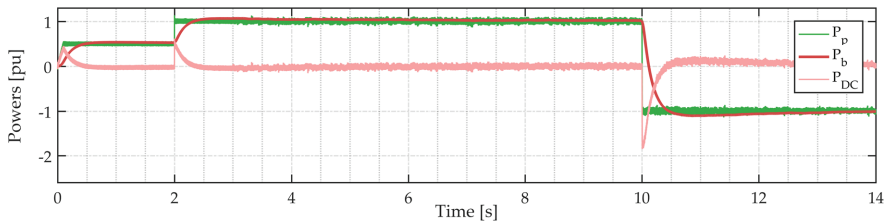**Figure 17.** Active and reactive power profiles of the smart grid.

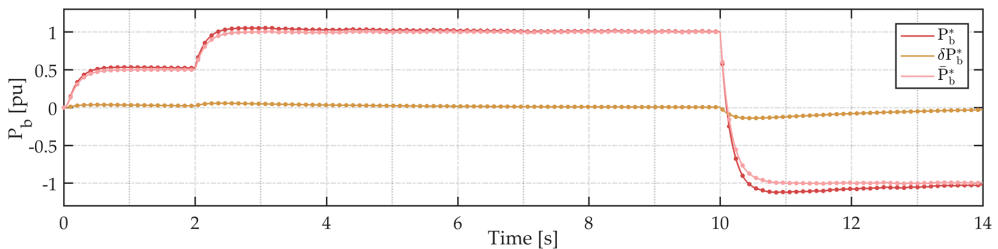**Figure 18.** Active powers: P_P (green), P_b (red), and P_{DC} (pink).

Figure 19. Reference active power components provided by BP: P_b^* (red), δP_b^* (gold), and $\bar{P}_b^*$ (pink).

Focusing now on the BP reference power profile, it is made up of two contributions, as pointed out in **Figure 19**: one comes from the low-pass filter ($\bar{P}_b^*$), whereas the other contribution (δP_b^*) is provided by a DC-link energy loop similar to that shown in **Figure 10**. Particularly, δP_b* enables BP to slowly drive the UM energy to a suitable intermediate reference value, as shown in **Figure 20**. This occurs by varying V_u and V suitably, as highlighted in **Figure 21**. It is worth noting that UM may be fully charged or discharged if this control loop is not employed and, thus, unable to cope with fast active power decrease or increase, respectively. In addition, δP_b^* accounts also for system losses that, if ignored, would force UM to be fully discharged. In conclusion, it is also worthy of note that reactive power variations do not affect both BP and UM power profiles significantly, as highlighted by the comparison between **Figure 17** and **Figure 18**.
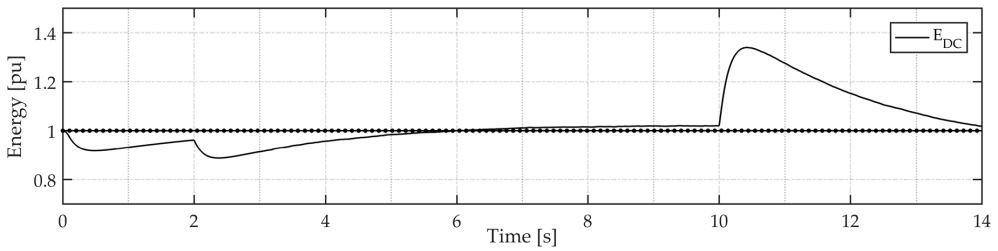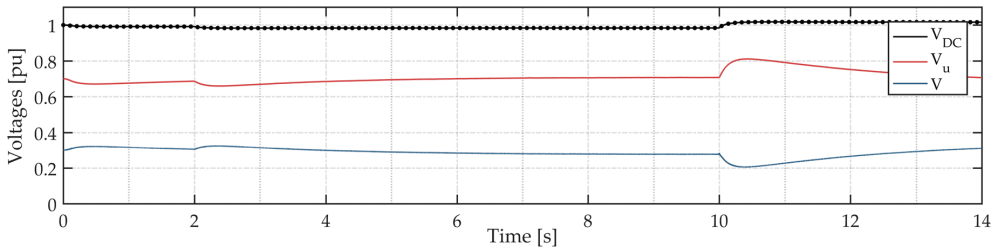
Figure 20. DC-link energy variations.

Figure 21. DC-link voltages: V_{DC} (gray), V_u (red), and V (blue).

4. Conclusion

This chapter has addressed the potentialities and advantages of a highly integrated battery-ultracapacitor system (HIBUC). Particularly, HIBUC benefits from the advantages of both passive and active hybrid energy storage system (HESS) configurations, namely a relative simple structure and an effective energy flow management of both the battery pack (BP) and the ultracapacitor module (UM). This has been proved by the analytical comparison among all the above-mentioned configurations, which reveals HIBUC as a very suitable and competitive solution, especially when high UM capacitance is concerned. In addition, HIBUC is also very flexible, as proved by the two application examples, namely an electric propulsion system and a smart grid. For each of these, HIBUC management and control approaches have been presented and discussed, providing some simulation results as well. These highlight the high level of integration achieved in each application, especially in the design of the HIBUC management stage, which should be done in accordance with the specific application requirements.

Acknowledgements

Author details

Alessandro Serpi[1,2]*, Mario Porru[1,2] and Alfonso Damiano[1]

*Address all correspondence to: alessandro.serpi@diee.unica.it

1 Department of Electrical and Electronic Engineering, University of Cagliari, Cagliari, Italy

2 NEPSY srl, Cagliari, Italy

References

[1] Huggins RA. Energy Storage. Boston, MA: Springer US; 2010

[2] Barnes FS, Levine JG. Large Energy Storage Systems Handbook. Boca Raton, FL: CRC Press; 2011. 254p

[3] IEA (International Energy Agency). Technology Roadmaps—Energy Storage. 2014

[4] Apsley JM, Gonzalez-Villasenor A, Barnes M, Smith AC, Williamson S, Schuddebeurs JD, et al. Propulsion drive models for full electric marine propulsion systems. IEEE Transactions on Industry Applications. 2009 Mar;**45**(2):676-684

[5] Arboleya P, Bidaguren P, Armendariz U. Energy is on board: Energy storage and other alternatives in modern light railways. IEEE Electrification Magazine. 2016 Sep;**4**(3):30-41

[6] Abad G, editor. Power Electronics and Electric Drives for Traction Applications. 1st ed. Chichester, UK: Wiley; 2016. 648p

[7] Tariq M, Maswood AI, Gajanayake CJ, Gupta AK. Aircraft batteries: Current trend towards more electric aircraft. IET Electrical Systems in Transportation. 2017;**7**(2):93-103

[8] Li R, Zhou F. Microgrid Technology and Engineering Application. Oxford, UK: Elsevier; 2015. 200p

[9] Gao DW. Energy Storage for Sustainable Microgrid. Oxford, UK: Academic Press; 2015. 153p

[10] Tan X, Li Q, Wang H. Advances and trends of energy storage technology in microgrid. International Journal of Electrical Power & Energy Systems. 2013 Jan;**44**(1):179-191

[11] Zakeri B, Syri S. Electrical energy storage systems: A comparative life cycle cost analysis. Renewable and Sustainable Energy Reviews. 2015 Feb;**42**:569-596

[12] Luo X, Wang J, Dooner M, Clarke J. Overview of current development in electrical energy storage technologies and the application potential in power system operation. Applied Energy. 2015 Jan;**137**:511-536

[13] Vazquez S, Lukic SM, Galvan E, Franquelo LG, Carrasco JM. Energy storage systems for transport and grid applications. IEEE Transactions on Industrial Electronics. 2010 Dec;**57**(12):3881-3895

[14] Boicea VA. Energy storage technologies: The past and the present. Proceedings of the IEEE. 2014 Nov;**102**(11):1777-1794

[15] Awadallah MA, Venkatesh B. Energy storage in flywheels: An overview. Canadian Journal of Electrical and Computer Engineering. 2015 Spring;**38**(2):183-193

[16] Gayathri NS, Senroy N, Kar IN. Smoothing of wind power using flywheel energy storage system. IET Renewable Power Generation. 2017;**11**(3):289-298

[17] Gee AM, Dunn RW. Analysis of trackside flywheel energy storage in light rail systems. IEEE Transactions on Vehicular Technology. 2015 Sep;**64**(9):3858-3869

[18] Ali MH, Wu B, Dougal RA. An overview of SMES applications in power and energy systems. IEEE Transactions on Sustainable Energy. 2010 Apr;**1**(1):38-47

[19] Liu Y, Tang Y, Shi J, Shi X, Deng J, Gong K. Application of small-sized SMES in an EV charging station with DC bus and PV system. IEEE Transactions on Applied Superconductivity. 2015 Jun;**25**(3):1-6

[20] Song M, Shi J, Liu Y, Xu Y, Hu N, Tang Y, et al. 100 kJ/50 kW HTS SMES for micro-grid. IEEE Transactions on Applied Superconductivity. 2015 Jun;**25**(3):1-6

[21] Grbovic PJ. Ultra-Capacitors in Power Conversion Systems: Applications, Analysis, and Design from Theory to Practice. Chichester, UK: Wiley-IEEE Press; 2014. 336p

[22] Jayasinghe SDG, Vilathgamuwa DM. Flying supercapacitors as power smoothing elements in wind generation. IEEE Transactions on Industrial Electronics. 2013 Jul;**60**(7): 2909-2918

[23] de la Torre S, Sánchez-Racero AJ, Aguado JA, Reyes M, Martínez O. Optimal sizing of energy storage for regenerative braking in electric railway systems. IEEE Transactions on Power Apparatus and Systems. 2015 May;**30**(3):1492-1500

[24] Aktas A, Erhan K, Ozdemir S, Ozdemir E. Experimental investigation of a new smart energy management algorithm for a hybrid energy storage system in smart grid applications. Electric Power Systems Research. 2017 Mar 1;**144**:185-196

[25] Hannan MA, Hoque MM, Mohamed A, Ayob A. Review of energy storage systems for electric vehicle applications: Issues and challenges. Renewable and Sustainable Energy Reviews. 2017 Mar 1;**69**:771-789

[26] Chong LW, Wong YW, Rajkumar RK, Rajkumar RK, Isa D. Hybrid energy storage systems and control strategies for stand-alone renewable energy power systems. Renewable and Sustainable Energy Reviews. 2016 Dec;**66**:174-189

[27] Zimmermann T, Keil P, Hofmann M, Horsche MF, Pichlmaier S, Jossen A. Review of system topologies for hybrid electrical energy storage systems. Journal of Energy Storage. 2016 Nov;**8**:78-90

[28] Dougal RA, Liu S, White RE. Power and life extension of battery-ultracapacitor hybrids. IEEE Transactions on Components and Packaging Technologies. 2002 Mar;**25**(1):120-131

[29] Gao L, Dougal RA, Liu S. Power enhancement of an actively controlled battery/ ultracapacitor hybrid. IEEE Transactions on Power Electronics. 2005 Jan;**20**(1):236-243

[30] Lukic SM, Cao J, Bansal RC, Rodriguez F, Emadi A. Energy storage systems for automotive applications. IEEE Transactions on Industrial Electronics. 2008 Jun;**55**(6):2258-2267

[31] Porru M, Serpi A, Marongiu I, Damiano A. A novel hybrid energy storage system for electric vehicles. In: Proceedings of the 41th Annual Conference of the IEEE Industrial Electronics Society (IECON 2015); Yokohama, Japan; 2015. pp. 3732-3737

[32] Porru M, Serpi A, Damiano A. Smart energy management of HESS-based electric propulsion systems for urban mobility. In: Proceedings of the 42nd Annual Conference of the IEEE Industrial Electronics Society (IECON 2016); Florence, Italy; 2016. pp. 4453-4458

[33] Porru M. Management and Control of Energy Storage Systems for Stationary and Automotive Applications [Internet] [PhD Dissertation] [Italy]. Department of Electrical and Electronic Engineering, University of Cagliari; 2015. Available from: http://veprints.unica.it/1117/

[34] Ma T, Yang H, Lu L. Development of hybrid battery–supercapacitor energy storage for remote area renewable energy systems. Applied Energy. 2015 Sep 1;**153**:56-62

[35] Pagano M, Piegari L. Hybrid electrochemical power sources for onboard applications. IEEE Transactions on Energy Conversion. 2007 Jun;**22**(2):450-456

[36] Wang B, Xu J, Cao B, Ning B. Adaptive mode switch strategy based on simulated annealing optimization of a multi-mode hybrid energy storage system for electric vehicles. Applied Energy. 2017 May 15;**194**:596-608

[37] Min H, Lai C, Yu Y, Zhu T, Zhang C. Comparison study of two semi-active hybrid energy storage Systems for hybrid electric vehicle applications and their experimental validation. Energies. 2017 Feb 28;**10**(3):279

[38] Song Z, Hofmann H, Li J, Han X, Zhang X, Ouyang M. A comparison study of different semi-active hybrid energy storage system topologies for electric vehicles. Journal of Power Sources. 2015 Jan 15;**274**:400-411

[39] Hredzak B, Agelidis VG, Jang M. A model predictive control system for a hybrid battery-ultracapacitor power source. IEEE Transactions on Power Electronics. 2014 Mar;**29**(3): 1469-1479

[40] Choi M-E, Kim S-W, Seo S-W. Energy management optimization in a battery/supercapacitor hybrid energy storage system. IEEE Transactions on Smart Grid. 2012 Mar;**3**(1):463-472

[41] Tankari MA, Camara MB, Dakyo B, Lefebvre G. Use of ultracapacitors and batteries for efficient energy management in wind-diesel hybrid system. IEEE Transactions on Sustainable Energy. 2013 Apr;**4**(2):414-424

[42] Bellache K, Camara MB, Dakyo B. Transient power control for diesel-generator assistance in electric boat applications using supercapacitors and batteries. IEEE Journal of Emerging and Selected Topics in Power Electronics. 2017;**PP**(99):1

[43] Araújo RE, de CR, Pinto C, Melo P, Freitas D. Combined sizing and energy management in EVs with batteries and supercapacitors. IEEE Transactions on Vehicular Technology. 2014 Sep;**63**(7):3062-3076

[44] Mendis N, Muttaqi KM, Perera S. Management of battery-supercapacitor hybrid energy storage and synchronous condenser for isolated operation of PMSG based variable-speed wind turbine generating systems. IEEE Transactions on Smart Grid. 2014 Mar;**5**(2):944-953

[45] Kollimalla SK, Mishra MK, Narasamma NL. Design and analysis of novel control strategy for battery and supercapacitor storage system. IEEE Transactions on Sustainable Energy. 2014 Oct;**5**(4):1137-1144

[46] Zeng A, Xu Q, Ding M, Yukita K, Ichiyanagi K. A classification control strategy for energy storage system in microgrid. IEEJ Transactions on Electrical and Electronic Engineering. 2015 Jul;**10**(4):396-403

[47] Wang G, Ciobotaru M, Agelidis VG. Power smoothing of large solar PV plant using hybrid energy storage. IEEE Transactions on Sustainable Energy. 2014 Jul;**5**(3):834-842

[48] Tummuru NR, Mishra MK, Srinivas S. Dynamic energy management of renewable grid integrated hybrid energy storage system. IEEE Transactions on Industrial Electronics. 2015 Dec;**62**(12):7728-7737

[49] Ye Y, Sharma R, Garg P. An integrated power management strategy of hybrid energy storage for renewable application. In: Proceedings of the 40th Annual Conference of the IEEE Industrial Electronics Society (IECON 2014); Dallas, USA; 2014. pp. 3088-3093

[50] Wang S, Tang Y, Shi J, Gong K, Liu Y, Ren L, et al. Design and advanced control strategies of a hybrid energy storage system for the grid integration of wind power generations. IET Renewable Power Generation. 2015 Feb;**9**(2):89-98

[51] Mohamed A, Salehi V, Mohammed O. Real-time energy management algorithm for mitigation of pulse loads in hybrid microgrids. IEEE Transactions on Smart Grid. 2012 Dec;**3**(4):1911-1922

[52] Garcia-Torres F, Bordons C. Optimal economical schedule of hydrogen-based microgrids with hybrid storage using model predictive control. IEEE Transactions on Industrial Electronics. 2015 Aug;**62**(8):5195-5207

[53] Laldin O, Moshirvaziri M, Trescases O. Predictive algorithm for optimizing power flow in hybrid ultracapacitor/battery storage systems for light electric vehicles. IEEE Transactions on Power Electronics. 2013 Agosto;**28**(8):3882-3895

[54] Larsson V, Johannesson L, Egardt B. Analytic solutions to the dynamic programming subproblem in hybrid vehicle energy management. IEEE Transactions on Vehicular Technology. 2015 Apr;**64**(4):1458-1467

[55] Shen J, Khaligh A. A supervisory energy management control strategy in a battery/ ultracapacitor hybrid energy storage system. IEEE Transactions on Transportation Electrification. 2015 Ottobre;**1**(3):223-231

[56] Herrera V, Gaztanaga H, Milo A, Saez-de-Ibarra A, Etxeberria I, Nieva T. Optimal energy management of battery-supercapacitor based light rail vehicle using genetic algorithms. IEEE Transactions on Industry Applications. 2016;**PP**(99):1

[57] Rouholamini M, Mohammadian M. Heuristic-based power management of a grid-connected hybrid energy system combined with hydrogen storage. Renewable Energy. 2016 Oct;**96**(Part A):354-365

[58] García-Triviño P, Llorens-Iborra F, García-Vázquez CA, Gil-Mena AJ, Fernández-Ramírez LM, Jurado F. Long-term optimization based on PSO of a grid-connected renewable energy/battery/hydrogen hybrid system. International Journal of Hydrogen Energy. 2014 Jul 15;**39**(21):10805-10816

[59] Porru M, Serpi A, Marongiu I, Damiano A. An improved DC-link voltage equalization for three-level neutral-point clamped converters. In: Proceedings of the 10th Conference on PhD Research in Microelectronics and Electronics (PRIME 2014); Grenoble, France; 2014. pp. 1-4

[60] Porru M, Serpi A, Marongiu I, Damiano A. A novel DC-link voltage and current control algorithm for neutral-point-clamped converters. In: Proceedings of the 40th Annual Conference of the IEEE Industrial Electronics Society (IECON 2014); Dallas, USA; 2014. pp. 4521-4527

[61] Porru M, Serpi A, Salimbeni, A., Damiano, A. An advanced frequency-based energy management of hybrid energy storage systems for microgrids. In: Proceedings of the 43rd Annual Conference of the IEEE Industrial Electronics Society (IECON 2017); Beijing, China; 2017